Adaptive Discontinuous Galerkin Finite Element Methods with Interior Penalty for the Compressible Navier–Stokes Equations

Ralf Hartmann[1] and Paul Houston[2]

[1] Institute of Aerodynamics and Flow Technology, German Aerospace Center, Lilienthalplatz 7, 38108 Braunschweig, Germany. Email: *Ralf.Hartmann@dlr.de*

[2] Department of Mathematics, University of Leicester, Leicester LE1 7RH, UK. Email: *Paul.Houston@mcs.le.ac.uk*. Supported by the EPSRC (Grant GR/R76615)

1 Introduction

In recent years there has been tremendous interest in the design of discontinuous Galerkin finite element methods (DGFEM) for the discretization of compressible fluid flow problems; see, for example, [2, 3, 6, 7] and the references cited therein. The key advantages of these schemes are that DGFEM provide robust and high-order accurate approximations, particularly in transport-dominated regimes, and that they are considerably flexible in the choice of mesh design. Indeed, DGFEM can easily handle non-matching grids and non-uniform, even anisotropic, polynomial approximation degrees.

In this paper we introduce the symmetric version of the interior penalty DGFEM for the numerical approximation of the compressible Navier–Stokes equations. We then consider the a posteriori error analysis and adaptive mesh design for the underlying discretization method. In particular, here we focus on so–called 'goal–oriented' a posteriori error estimation which bounds the error measured in terms of certain target functionals of real or physical interest. Typical examples that we shall consider here include the drag and lift coefficients of a body immersed in a viscous fluid. By employing a duality argument we derive a weighted (Type I) a posteriori error bound which reflects the error creation and error propagation mechanisms inherent in viscous compressible fluid flows. On the basis of this a posteriori estimate, we design and implement the corresponding adaptive algorithm to ensure both the reliable and efficient control of the error in the prescribed target functional. The superiority of the proposed approach over standard mesh refinement algorithms which employ empirical error indicators will be demonstrated. This paper represents a continuation of our previous work presented in the articles [10, 11].

2 The compressible Navier-Stokes equations

Writing ρ, $\mathbf{v} = (v_1, v_2)^T$, p, E and T to denote the density, velocity vector, pressure, specific total energy and temperature, respectively, the equations are given by

$$\nabla \cdot (\mathcal{F}^c(\mathbf{u}) - \mathcal{F}^v(\mathbf{u}, \nabla\mathbf{u})) \equiv \sum_{i=1}^{2} \frac{\partial}{\partial x_i}\mathbf{f}_i^c(\mathbf{u}) - \sum_{i=1}^{2} \frac{\partial}{\partial x_i}\mathbf{f}_i^v(\mathbf{u}, \nabla\mathbf{u}) = \mathbf{0} \quad \text{in } \Omega, \tag{1}$$

where Ω is an open bounded domain in $\mathbb{R}^2$. Here, the vector of conservative variables $\mathbf{u}$, the convective fluxes $\mathbf{f}_i^c$, $i = 1, 2$, and the viscous fluxes $\mathbf{f}_i^v$, $i = 1, 2$, are defined by $\mathbf{u} = [\rho, \rho v_1, \rho v_2, \rho E]^T$, $\mathbf{f}_i^c(\mathbf{u}) = [\rho v_i, \rho v_1 v_i + \delta_{1i} p, \rho v_2 v_i + \delta_{2i} p, \rho H v_i]^T$ and

$\mathbf{f}_i^v = [0, \tau_{1i}, \tau_{2i}, \tau_{i1}v_1 + \tau_{i2}v_2 + \mathcal{K}T_{x_i}]^T$, respectively. Here, $\mathcal{K}$ is the thermal conductivity coefficient and H is the total enthalpy defined by $H = E + p/\rho$. The pressure is determined by the equation of state of an ideal gas, i.e., $p = (\gamma - 1)\rho(E - \frac{1}{2}\mathbf{v}^2)$, where $\gamma = c_p/c_v$ is the ratio of specific heat capacities; for dry air, $\gamma = 1.4$. For a Newtonian fluid, the viscous stress tensor is given by $\tau = \mu\left(\nabla\mathbf{v} + (\nabla\mathbf{v})^T - \frac{2}{3}(\nabla\cdot\mathbf{v})I\right)$, where μ is the dynamic viscosity coefficient; the temperature T is given by $\mathcal{K}T = \frac{\mu\gamma}{Pr}\left(E - \frac{1}{2}\mathbf{v}^2\right)$, where $\mathrm{Pr} = 0.72$ is the Prandtl number.

The non-dimensionalized form of the Navier–Stokes equations (1) are given by

$$\nabla\cdot\mathcal{F}^c(\mathbf{u}) - \nabla\cdot(G_{1j}\partial\mathbf{u}/\partial x_j, G_{2j}\partial\mathbf{u}/\partial x_j) = \mathbf{0} \quad \text{in } \Omega, \tag{2}$$

where repeated indices are summed through their range. Here, the matrices $G_{ij} = \partial\mathbf{f}_i^v(\mathbf{u},\nabla\mathbf{u})/\partial u_{x_j}$, for $i,j = 1,2$, i.e., $\mathbf{f}_i^v(\mathbf{u},\nabla\mathbf{u}) = \sum_{j=1}^2 G_{ij}\partial\mathbf{u}/\partial x_j$, $i = 1,2$, where

$$G_{11} = \frac{1}{\rho\,\mathrm{Re}}\begin{pmatrix} 0 & 0 & 0 & 0 \\ -\frac{4}{3}v_1 & \frac{4}{3} & 0 & 0 \\ -v_2 & 0 & 1 & 0 \\ -\left(\frac{4}{3}v_1^2 + v_2^2 + \frac{\gamma}{\mathrm{Pr}}\left(E - \mathbf{v}^2\right)\right) & \left(\frac{4}{3} - \frac{\gamma}{\mathrm{Pr}}\right)v_1 & \left(1 - \frac{\gamma}{\mathrm{Pr}}\right)v_2 & \frac{\gamma}{\mathrm{Pr}} \end{pmatrix},$$

$$G_{12} = \frac{1}{\rho\,\mathrm{Re}}\begin{pmatrix} 0 & 0 & 0 & 0 \\ \frac{2}{3}v_2 & 0 & -\frac{2}{3} & 0 \\ -v_1 & 1 & 0 & 0 \\ -\frac{1}{3}v_1v_2 & v_2 & -\frac{2}{3}v_1 & 0 \end{pmatrix}, G_{21} = \frac{1}{\rho\,\mathrm{Re}}\begin{pmatrix} 0 & 0 & 0 & 0 \\ -v_2 & 0 & 1 & 0 \\ \frac{2}{3}v_1 & -\frac{2}{3} & 0 & 0 \\ -\frac{1}{3}v_1v_2 & -\frac{2}{3}v_2 & v_1 & 0 \end{pmatrix},$$

$$G_{22} = \frac{1}{\rho\,\mathrm{Re}}\begin{pmatrix} 0 & 0 & 0 & 0 \\ -v_1 & 1 & 0 & 0 \\ -\frac{4}{3}v_2 & 0 & \frac{4}{3} & 0 \\ -\left(v_1^2 + \frac{4}{3}v_2^2 + \frac{\gamma}{\mathrm{Pr}}\left(E - \mathbf{v}^2\right)\right) & \left(1 - \frac{\gamma}{\mathrm{Pr}}\right)v_1 & \left(\frac{4}{3} - \frac{\gamma}{\mathrm{Pr}}\right)v_2 & \frac{\gamma}{\mathrm{Pr}} \end{pmatrix},$$

and Re denotes the Reynolds number.

Given that $\Omega \subset \mathbb{R}^2$ is a bounded region, with boundary Γ, the system of conservation laws (2) must be supplemented by appropriate boundary conditions. For simplicity of presentation, we assume that Γ may be decomposed as follows $\Gamma = \Gamma_{\mathrm{D}} \cup \Gamma_{\mathrm{N,sup}} \cup \Gamma_{\mathrm{N,sub}} \cup \Gamma_{\mathrm{W}}$, where Γ_{D}, $\Gamma_{\mathrm{N,sup}}$, $\Gamma_{\mathrm{N,sub}}$ and Γ_{W} are distinct subsets of Γ representing the Dirichlet (inflow), Neumann (supersonic-outflow), Neumann (subsonic-outflow) and solid wall boundaries, respectively. Thereby, we may specify the following boundary conditions: $\mathbf{u} = \mathbf{u}_D$ on Γ_{D}, $\mathcal{F}^v(\mathbf{u},\nabla\mathbf{u})\cdot\mathbf{n} = \mathbf{0}$ on $\Gamma_{\mathrm{N,sup}} \cup \Gamma_{\mathrm{N,sub}}$; note that on $\Gamma_{\mathrm{N,sub}}$ an additional condition which imposes a given pressure p_{out} is enforced. For solid wall boundaries, we consider the distinction between *isothermal* and *adiabatic* conditions. To this end, decomposing $\Gamma_W = \Gamma_{\mathrm{W,iso}} \cup \Gamma_{\mathrm{W,adia}}$, we set $\mathbf{v} = \mathbf{0}$ on Γ_{W}, $T = T_{\mathrm{wall}}$ on $\Gamma_{\mathrm{W,iso}}$, $\mathbf{n}\cdot\nabla T = 0$ on $\Gamma_{\mathrm{W,adia}}$, where T_{wall} is a given wall temperature; we refer to [2, 3, 5, 6] and the references cited therein for further details concerning the imposition of suitable boundary conditions.

3 Discontinuous Galerkin Discretization

In this section we introduce the discontinuous Galerkin method with interior penalty for the discretization of the compressible Navier–Stokes equations (2).

We assume that Ω can be subdivided into shape-regular meshes $\mathcal{T}_h = \{\kappa\}$ consisting of quadrilateral elements κ. For each $\kappa \in \mathcal{T}_h$, we denote by $\mathbf{n}_\kappa$ the unit outward normal vector to the boundary $\partial\kappa$, and by h_κ the elemental diameter. An interior edge of $\mathcal{T}_h$ is the (non-empty) one-dimensional interior of $\partial\kappa^+ \cap \partial\kappa^-$, where κ^+ and κ^- are two adjacent elements of $\mathcal{T}_h$. Similarly, a boundary edge of $\mathcal{T}_h$ is the (non-empty) one-dimensional interior of $\partial\kappa \cap \Gamma$ which consists of entire edges of $\partial\kappa$. We denote by $\mathcal{E}_{\mathcal{I}}$ the union of all interior edges of $\mathcal{T}_h$, by $\mathcal{E}_\Gamma$ the union of all boundary edges, and set $\mathcal{E} = \mathcal{E}_{\mathcal{I}} \cup \mathcal{E}_\Gamma$.

Next, we define average and jump operators. To this end, let κ^+ and κ^- be two adjacent elements of $\mathcal{T}_h$ and $\mathbf{x}$ be an arbitrary point on the interior edge $e = \partial\kappa^+ \cap \partial\kappa^- \subset \mathcal{E}_{\mathcal{I}}$. Moreover, let $\mathbf{v}$ and $\underline{\tau}$ be vector- and matrix-valued functions, respectively, that are smooth inside each element $\kappa^\pm$. By $(\mathbf{v}^\pm, \underline{\tau}^\pm)$ we denote the traces of $(\mathbf{v}, \underline{\tau})$ on e taken from within the interior of $\kappa^\pm$, respectively. Then, we define the averages at $\mathbf{x} \in e$ by $\{\!\{\mathbf{v}\}\!\} = (\mathbf{v}^+ + \mathbf{v}^-)/2$ and $\{\!\{\underline{\tau}\}\!\} = (\underline{\tau}^+ + \underline{\tau}^-)/2$. Similarly, the jumps at $\mathbf{x} \in e$ are given by $\underline{[\![\mathbf{v}]\!]} = \mathbf{v}^+ \otimes \mathbf{n}_{\kappa^+} + \mathbf{v}^- \otimes \mathbf{n}_{\kappa^-}$ and $[\![\underline{\tau}]\!] = \underline{\tau}^+ \cdot \mathbf{n}_{\kappa^+} + \underline{\tau}^- \cdot \mathbf{n}_{\kappa^-}$. For matrices $\underline{\sigma}, \underline{\tau} \in \mathbb{R}^{m\times n}$, $m, n \geq 1$, we use the standard notation $\underline{\sigma} : \underline{\tau} = \sum_{k=1}^{m}\sum_{l=1}^{n} \sigma_{kl}\tau_{kl}$; additionally, for vectors $\mathbf{v} \in \mathbb{R}^m, \mathbf{w} \in \mathbb{R}^n$, the matrix $\mathbf{v} \otimes \mathbf{w} \in \mathbb{R}^{m\times n}$ is defined by $(\mathbf{v} \otimes \mathbf{w})_{kl} = v_k w_l$.

Given a polynomial degree $p \geq 1$, we define the finite element space $\mathbf{V}_h = \{\mathbf{v} \in [L_2(\Omega)]^4 : \mathbf{v}|_\kappa \in [\mathcal{Q}_p(\kappa)]^4,\ \kappa \in \mathcal{T}_h\}$, where $\mathcal{Q}_p(\kappa)$ denotes the space of tensor product polynomials on κ of degree p in each coordinate direction. We consider the following interior penalty discontinuous Galerkin discretization of equations (2): find $\mathbf{u}_h \in \mathbf{V}_h$ such that

$$
\begin{aligned}
\mathcal{N}(\mathbf{u}_h, \mathbf{v}_h) &\equiv -\int_\Omega \mathcal{F}^c(\mathbf{u}_h) : \nabla_h \mathbf{v}_h \,\mathrm{d}\mathbf{x} + \sum_{\kappa\in\mathcal{T}_h} \int_{\partial\kappa\setminus\Gamma} \mathcal{H}(\mathbf{u}_h^+, \mathbf{u}_h^-, \mathbf{n}_\kappa) \cdot \mathbf{v}_h^+ \,\mathrm{d}s \\
&+ \int_\Omega \mathcal{F}^v(\mathbf{u}_h, \nabla_h \mathbf{u}_h) : \nabla_h \mathbf{v}_h \,\mathrm{d}\mathbf{x} - \int_{\mathcal{E}_{\mathcal{I}}} \{\!\{\mathcal{F}^v(\mathbf{u}_h, \nabla_h \mathbf{u}_h)\}\!\} : \underline{[\![\mathbf{v}_h]\!]} \,\mathrm{d}s \\
&- \int_{\mathcal{E}_{\mathcal{I}}} \{\!\{ \left(G_{i1}^T \partial_h \mathbf{v}_h/\partial x_i, G_{i2}^T \partial_h \mathbf{v}_h/\partial x_i\right) \}\!\} : \underline{[\![\mathbf{u}_h]\!]})\,\mathrm{d}s + \int_{\mathcal{E}_{\mathcal{I}}} \Sigma \underline{[\![\mathbf{u}_h]\!]} : \underline{[\![\mathbf{v}_h]\!]} \,\mathrm{d}s + \mathcal{N}_\Gamma(\mathbf{u}_h, \mathbf{v}_h) = 0 \quad (3)
\end{aligned}
$$

for all $\mathbf{v}_h$ in $\mathbf{V}_h$. Here, the subscript h on the operators ∇_h and $\partial_h/\partial x_i$, $i = 1, 2$, is used to denote the discrete counterparts of ∇ and $\partial/\partial x_i$, $i = 1, 2$, respectively, taken elementwise. Furthermore, $\mathcal{H}(\cdot, \cdot, \cdot)$ denotes a *numerical (convective) flux* function, assumed to be Lipschitz continuous, consistent and conservative. The function $\Sigma \in L^\infty(\mathcal{E})$ denotes the so–called discontinuity penalization function; defining $\mathtt{h} \in L^\infty(\mathcal{E})$ by $\mathtt{h}(\mathbf{x}) = \min\{h_{\kappa^+}, h_{\kappa^-}\}$ when $\mathbf{x} \in e = \partial\kappa^+ \cap \partial\kappa^- \subset \mathcal{E}_{\mathcal{I}}$, and $\mathtt{h}(\mathbf{x}) = h_\kappa$ when $\mathbf{x} \in e = \partial\kappa \cap \Gamma \subset \mathcal{E}_\Gamma$, we set $\Sigma = C_\Sigma/(\mathtt{h}\,\mathrm{Re})$, with a parameter $C_\Sigma > 0$ that is independent of $\mathtt{h}$. Finally, we write

$$
\begin{aligned}
\mathcal{N}_\Gamma(\mathbf{u}_h, \mathbf{v}_h) &= \int_\Gamma \mathcal{H}(\mathbf{u}_h^+, \mathbf{u}_\Gamma(\mathbf{u}_h^+), \mathbf{n}) \cdot \mathbf{v}_h^+ \,\mathrm{d}s + \int_{\Gamma_{\mathrm{D}}\cup\Gamma_{\mathrm{W}}} \Sigma \left(\mathbf{u}_h^+ - \mathbf{u}_\Gamma(\mathbf{u}_h^+)\right) \cdot \mathbf{v}_h^+ \,\mathrm{d}s, \\
&- \int_{\Gamma_{\mathrm{D}}\cup\Gamma_{\mathrm{W,iso}}} \mathcal{F}^v(\mathbf{u}_h, \nabla_h \mathbf{u}_h) : \mathbf{v}_h^+ \otimes \mathbf{n} \,\mathrm{d}s - \int_{\Gamma_{\mathrm{W,adia}}} \hat{\mathcal{F}}^v(\mathbf{u}_h, \nabla_h \mathbf{u}_h) : \mathbf{v}_h^+ \otimes \mathbf{n} \,\mathrm{d}s \\
&- \int_{\Gamma\setminus\Gamma_{\mathrm{N,sup}}} \left(G_{i1}^T(\mathbf{u}_h^+) \partial_h \mathbf{v}_h^+/\partial x_i, G_{i2}^T(\mathbf{u}_h^+) \partial_h \mathbf{v}_h^+/\partial x_i\right) : \left(\mathbf{u}_h^+ - \mathbf{u}_\Gamma(\mathbf{u}_h^+)\right) \otimes \mathbf{n} \,\mathrm{d}s,
\end{aligned}
$$

where the boundary function $\mathbf{u}_\Gamma(\mathbf{u})$ is given according to the type of boundary condition imposed. We set $\mathbf{u}_\Gamma(\mathbf{u}) = \mathbf{u}_D$ on Γ_{D}, $\mathbf{u}_\Gamma(\mathbf{u}) = \mathbf{u}$ on $\Gamma_{\mathrm{N,sup}}$, and $\mathbf{u}_\Gamma(\mathbf{u}) = (\rho, \rho v_1, \rho v_2, \frac{p_{\mathrm{out}}}{\gamma-1} + \frac{1}{2}\rho\mathbf{v}^2)^T$ on $\Gamma_{\mathrm{N,sub}}$. Furthermore, we set $\mathbf{u}_\Gamma(\mathbf{u}) = (\rho, 0, 0, \rho c_v T_{\mathrm{wall}})^T$ on $\Gamma_{\mathrm{W,iso}}$, and $u_\Gamma(\mathbf{u}) = (\rho, 0, 0, \frac{p}{\gamma-1})^T = (\rho, 0, 0, \rho E - \frac{1}{2}\rho\mathbf{v}^2)^T$ on $\Gamma_{\mathrm{W,adia}}$. Finally, we note that on the adiabatic boundary $\Gamma_{\mathrm{W,adia}}$, we define $\hat{\mathcal{F}}^v(\mathbf{u}, \nabla\mathbf{u})$ such that

$$
\hat{\mathcal{F}}^v(\mathbf{u}, \nabla\mathbf{u}) \cdot \mathbf{n} = (0, \tau_{11}n_1 + \tau_{12}n_2, \tau_{21}n_1 + \tau_{22}n_2, 0)^T.
$$

Remark 1. We remark that the discretization of the viscous terms has been done by employing the symmetric version of the interior penalty method, cf. [1], and the references cited therein. In particular, we note that this scheme is derived by first re-writing (2) as a system of first–order partial differential equations through the introduction of appropriate auxiliary variables. By defining suitable numerical flux functions, these additional variables are subsequently eliminated; see [1, 8] for details. We note that within this process the transpose of the matrices G_{ij}, $i, j = 1, 2$, naturally arise in the definition of the DGFEM. Moreover, this is necessary to ensure the adjoint consistency of the resulting method which is essential for the approximation of functionals of the solution, cf. [1, 8]. As a final remark, we note that the discontinuity penalization parameter Σ must be chosen sufficiently large in order to guarantee the stability of the underlying method.

4 Goal–oriented a posteriori error estimation

In this section, we shall be concerned with controlling the error in the numerical solution measured in terms of a given target functional $J(\cdot)$; for a detailed discussion, we refer to the review articles [4, 13]. Assuming that $J(\cdot)$ is differentiable, we write

$$\bar{J}(\mathbf{u}, \mathbf{u}_h; \mathbf{u} - \mathbf{u}_h) = J(\mathbf{u}) - J(\mathbf{u}_h) = \int_0^1 J'[\theta\mathbf{u} + (1-\theta)\mathbf{u}_h](\mathbf{u} - \mathbf{u}_h)\,\mathrm{d}\theta, \tag{4}$$

where $J'[\mathbf{w}](\cdot)$ denotes the Fréchet derivative of $J(\cdot)$ evaluated at some $\mathbf{w}$ in $\mathbf{V}$. Here, $\mathbf{V}$ is some suitably chosen function space such that $\mathbf{V}_h \subset \mathbf{V}$. Analogously, we write

$$\mathcal{M}(\mathbf{u}, \mathbf{u}_h; \mathbf{u} - \mathbf{u}_h, \mathbf{v}) = \mathcal{N}(\mathbf{u}, \mathbf{v}) - \mathcal{N}(\mathbf{u}_h, \mathbf{v}) = \int_0^1 \mathcal{N}'_{\mathbf{u}}[\theta\mathbf{u} + (1-\theta)\mathbf{u}_h](\mathbf{u} - \mathbf{u}_h, \mathbf{v})\,\mathrm{d}\theta \tag{5}$$

for all $\mathbf{v}$ in $\mathbf{V}$. Here, $\mathcal{N}'_{\mathbf{u}}[\mathbf{w}](\cdot, \mathbf{v})$ denotes the Fréchet derivative of $\mathbf{u} \mapsto \mathcal{N}(\mathbf{u}, \mathbf{v})$, for $\mathbf{v} \in \mathbf{V}$ fixed, at some $\mathbf{w}$ in $\mathbf{V}$. We remark that the linearization defined in (5) is only a *formal* calculation, in the sense that $\mathcal{N}'_{\mathbf{u}}[\mathbf{w}](\cdot, \cdot)$ may not in general exist. Instead, a suitable approximation to $\mathcal{N}'_{\mathbf{u}}[\mathbf{w}](\cdot, \cdot)$ must be determined, for example, by computing appropriate finite difference quotients of $\mathcal{N}(\cdot, \cdot)$, cf. [9, 10]. Given a suitable linearization, we introduce the following *dual* problem: find $\mathbf{z} \in \mathbf{V}$ such that

$$\mathcal{M}(\mathbf{u}, \mathbf{u}_h; \mathbf{w}, \mathbf{z}) = \bar{J}(\mathbf{u}, \mathbf{u}_h; \mathbf{w}) \quad \forall \mathbf{w} \in \mathbf{V}. \tag{6}$$

We assume that (6) possesses a unique solution. Clearly, the validity of this assumption depends on both the definition of $\mathcal{M}(\mathbf{u}, \mathbf{u}_h; \cdot, \cdot)$ and the choice of the target functional under consideration, cf. [10]. For the proceeding error analysis, we must therefore *assume* that the dual problem (6) is well–posed.

Proposition 1. *Let $\mathbf{u}$ and $\mathbf{u}_h$ denote the solutions of (2) and (3), respectively, and suppose that the dual problem (6) is well–posed. Then,*

$$J(\mathbf{u}) - J(\mathbf{u}_h) \leq \sum_{\kappa \in \mathcal{T}_h} |\eta_\kappa|, \tag{7}$$

where

$$
\begin{aligned}
\eta_\kappa = &\int_\kappa \mathbf{R}_h \cdot \boldsymbol{\omega}_h \, d\mathbf{x} + \int_{\partial\kappa\setminus\Gamma} (\mathcal{F}^c(\mathbf{u}_h)\cdot\mathbf{n}_\kappa - \mathcal{H}(\mathbf{u}_h^+, \mathbf{u}_h^-, \mathbf{n}_\kappa)) \cdot \boldsymbol{\omega}_h^+ \, ds \\
&+ \int_{\partial\kappa\cap\Gamma} (\mathcal{F}^c(\mathbf{u}_h)\cdot\mathbf{n}_\kappa - \mathcal{H}(\mathbf{u}_h^+, \mathbf{u}_\Gamma(\mathbf{u}_h^+), \mathbf{n}_\kappa)) \cdot \boldsymbol{\omega}_h^+ \, ds - \int_{\partial\kappa\setminus\Gamma} \Sigma \underline{[\![\mathbf{u}_h]\!]} : \boldsymbol{\omega}_h^+ \otimes \mathbf{n}_\kappa \, ds \\
&+ \frac{1}{2}\int_{\partial\kappa\setminus\Gamma} \Big((G_{i1}^T \partial_h \boldsymbol{\omega}_h/\partial x_i, G_{i2}^T \partial_h \boldsymbol{\omega}_h/\partial x_i) : \underline{[\![\mathbf{u}_h]\!]} - [\![\mathcal{F}^v(\mathbf{u}_h, \nabla_h \mathbf{u}_h)]\!] \cdot \boldsymbol{\omega}_h^+ \Big) \, ds \\
&- \int_{\partial\kappa\cap(\Gamma_D\cup\Gamma_W)} \Sigma \left(\mathbf{u}_h^+ - \mathbf{u}_\Gamma(\mathbf{u}_h^+)\right) \cdot \boldsymbol{\omega}_h^+ \, ds \\
&- \int_{\partial\kappa\cap(\Gamma_{N,sub}\cup\Gamma_{N,sup})} (\mathcal{F}^v(\mathbf{u}_h^+, \nabla_h \mathbf{u}_h^+)\cdot\mathbf{n}_\kappa) \cdot \boldsymbol{\omega}_h^+ \, ds \\
&- \int_{\partial\kappa\cap\Gamma_{W,adia}} \Big(\mathcal{F}^v(\mathbf{u}_h^+, \nabla_h \mathbf{u}_h^+) - \hat{\mathcal{F}}^v(\mathbf{u}_h^+, \nabla_h \mathbf{u}_h^+)\Big) : \boldsymbol{\omega}_h^+ \otimes \mathbf{n} \, ds \\
&+ \int_{\partial\kappa\cap(\Gamma\setminus\Gamma_{N,sup})} (G_{i1}^T(\mathbf{u}_h^+) \partial_h \boldsymbol{\omega}_h^+/\partial x_i, G_{i2}^T(\mathbf{u}_h^+) \partial_h \boldsymbol{\omega}_h^+/\partial x_i) : \left(\mathbf{u}_h^+ - \mathbf{u}_\Gamma(\mathbf{u}_h^+)\right) \otimes \mathbf{n} \, ds,
\end{aligned}
$$

and $\boldsymbol{\omega}_h = \mathbf{z} - \mathbf{z}_h$ *for all* $\mathbf{z}_h$ *in* $\mathbf{V}_h$. *Here,* $\mathbf{R}_h|_\kappa = -\nabla_h \cdot \mathcal{F}^c(\mathbf{u}_h) + \nabla_h \cdot \mathcal{F}^v(\mathbf{u}_h, \nabla_h \mathbf{u}_h)$, $\kappa \in \mathcal{T}_h$, *denotes the elementwise residual.*

Proof. Choosing $\mathbf{w} = \mathbf{u} - \mathbf{u}_h$ in (6), recalling the linearization performed in (4), and exploiting the Galerkin orthogonality property of the DGFEM, we get

$$
\begin{aligned}
J(\mathbf{u}) - J(\mathbf{u}_h) &= \bar{J}(\mathbf{u}, \mathbf{u}_h; \mathbf{u} - \mathbf{u}_h) = \mathcal{M}(\mathbf{u}, \mathbf{u}_h; \mathbf{u} - \mathbf{u}_h, \mathbf{z}) \\
&= \mathcal{M}(\mathbf{u}, \mathbf{u}_h; \mathbf{u} - \mathbf{u}_h, \mathbf{z} - \mathbf{z}_h) = -\mathcal{N}(\mathbf{u}_h, \mathbf{z} - \mathbf{z}_h) \quad \forall \mathbf{z}_h \in \mathbf{V}_h.
\end{aligned}
$$

Equation (7) now follows by the divergence theorem together with the triangle inequality.

We end this section by noting that the Type I a posteriori error bound (7) depends on the unknown analytical solution to the primal and dual problems. Thus, in order to render these quantities computable, both $\mathbf{u}$ and $\mathbf{z}$ must be replaced by suitable approximations. Here, the linearizations leading to $\mathcal{M}(\mathbf{u}, \mathbf{u}_h; \cdot, \cdot)$ and $\bar{J}(\mathbf{u}, \mathbf{u}_h; \cdot)$ are performed about $\mathbf{u}_h$ and the dual solution $\mathbf{z}$ is replaced by a DGFEM approximation $\hat{\mathbf{z}}$ computed on the same mesh $\mathcal{T}_h$ used for $\mathbf{u}_h$, but with a higher degree polynomial.

5 Numerical example

In this section we present a numerical example to highlight the advantages of designing an adaptive finite element algorithm based on the weighted error indicator $|\eta_\kappa|$ in comparison with both uniform mesh refinement, as well as an adaptive algorithm based on an empirical refinement indicator which does not require the solution of an auxiliary (dual) problem; for simplicity, we employ a Type II residual indicator of the form derived in [10]. Throughout this section, we employ the Vijayasundaram flux for the discretization of the convective terms and set $p = 1$ (bilinear elements). Finally, for both adaptive refinement strategies, we use the fixed fraction refinement algorithm with refinement and derefinement fractions set to 20% and 10%, respectively; we also note that for the computation of $|\eta_\kappa|$, the dual solution is approximated using piecewise biquadratic polynomials.

We consider a Mach 0.8 flow at an angle of attack $\alpha = 10°$ with Reynolds number $\mathrm{Re} = 73$ and constant temperature on the profile, cf. [3, 12]. The solution to this problem

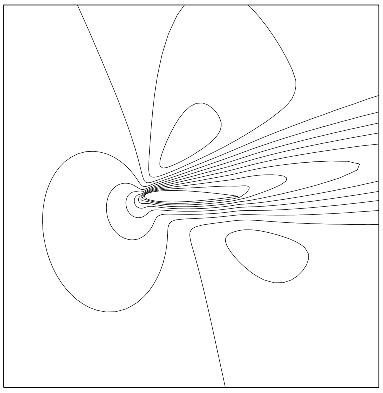

(a)

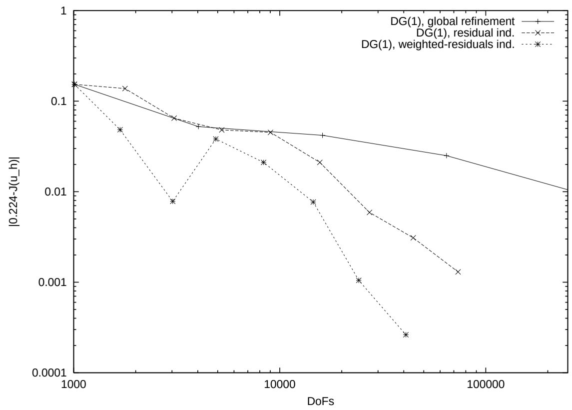

(b)

Fig. 1. (a) Mach isolines, $\mathrm{Ma} = \frac{i}{10}, i = 1, \ldots, 10$, of the flow around the NACA0012 airfoil; (b) Convergence of the error $|J(\mathbf{u}) - J(\mathbf{u}_h)|$ using each mesh refinement strategy.

Table 1. Adaptive algorithm based on the weighted error indicator $|\eta_\kappa|$.

Elements	DOF	$J(\mathbf{u}) - J(\mathbf{u}_h)$	$\sum_\kappa \eta_\kappa$	θ_1	$\sum_\kappa \lvert\eta_\kappa\rvert$	θ_2
63	1008	-1.534e-01	-1.299e-01	0.85	9.2e-01	6.02
105	1680	-4.838e-02	-1.114e-02	0.23	7.4e-01	15.35
189	3024	7.814e-03	5.574e-03	0.71	7.9e-01	100.60
306	4896	-3.819e-02	-1.296e-02	0.34	8.1e-01	21.11
522	8352	-2.107e-02	-9.249e-03	0.44	8.5e-01	40.25
909	14544	-7.686e-03	-3.746e-03	0.49	7.9e-01	102.9
1512	24192	-1.049e-03	-9.130e-04	0.87	1.0e+00	962
2559	40944	-2.628e-04	-2.395e-04	0.91	6.2e-01	2374

consists of a flow that is mainly subsonic with a small supersonic region above the airfoil, see Fig. 1(a). Here, we consider the evaluation of the inviscid drag coefficient (c_{dp}) on the surface of the airfoil. On the basis of a fine grid computation, the reference value of the functional is given by $J(\mathbf{u}) \approx 0.224$.

In Fig. 1(b) we compare the true error in the computed target functional $J(\cdot)$ using all three mesh refinement strategies. Here, we clearly observe the superiority of the weighted a posteriori error indicator; at all refinement steps the error in the computed functional is less than the corresponding quantity when either uniform refinement or adaptive refinement based on an empirical residual indicator is employed. Indeed, on the final mesh the true error in $J(\cdot)$ is over an order of magnitude smaller than $|J(\mathbf{u}) - J(\mathbf{u}_h)|$ computed on the sequence of meshes generated by the empirical indicator.

In Table 1 we collect the data of the adaptive algorithm when employing the weighted indicators. Here, we show the number of elements and degrees of freedom (DOF) in $\mathbf{V}_h$, the true error in the functional $J(\mathbf{u}) - J(\mathbf{u}_h)$, the computed error representation formula, the approximate a posteriori error bound and their respective effectivity indices $\theta_1 = \sum_\kappa \eta_\kappa / (J(\mathbf{u}) - J(\mathbf{u}_h))$ and $\theta_2 = \sum_\kappa |\eta_\kappa| / |J(\mathbf{u}) - J(\mathbf{u}_h)|$. First we note that on all refinement steps the correct sign of the error is predicted by the computed error representation formula. Furthermore, whereas on very coarse meshes the quality of $\sum_\kappa \eta_\kappa$

Table 2. Nonlinear Newton residuals (Res.) and convergence rates on a sequence of uniformly refined meshes. *: On the coarsest mesh only the last 4 out of 6 iteration steps are displayed.

Mesh 1		Mesh 2		Mesh 3		Mesh 4		Mesh 5	
Res.	Rate	Res.	Rate	Res.	Rate	Res.	Rate	Res.	Rate
6.5-02*	-	8.1-01	-	4.4-01	-	2.4-01	-	1.1-01	
2.5-02	3	4.2-02	19	3.3-02	13	1.6-02	16	5.9-03	19
6.7-04	37	1.2-03	36	1.6-03	20	2.6-04	62	1.4-04	43
6.6-07	1021	1.4-06	808	1.8-05	92	2.6-07	976	1.7-04	804
3.7-10	1755	3.1-10	4538	2.9-09	6199	5.5-11	4750	1.7-10	1021

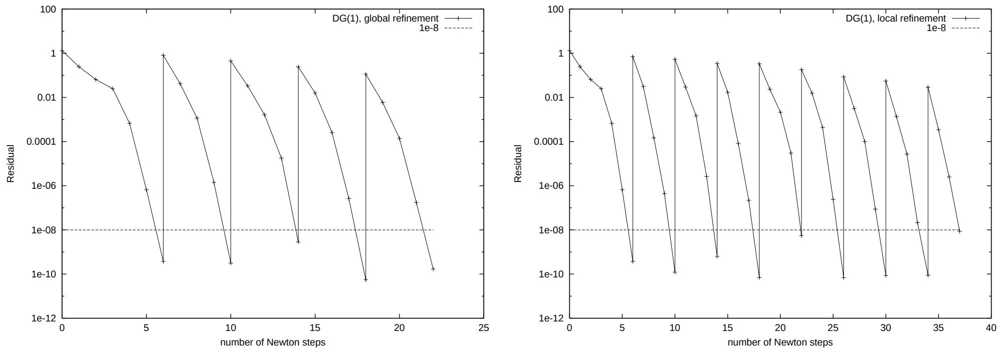

(a) (b)

Fig. 2. Convergence of the nonlinear residual with the number of Newton steps employed: (a) Uniform mesh refinement; (b) Adaptive mesh refinement using the empirical error indicator.

is rather poor, in the sense that θ_1 is noticeable smaller than one, we see that the effectivity indices θ_1 slowly tend towards unity as the mesh is refined. On the other hand, even just the application of the triangle inequality leads to significant over–estimation of the true error in the computed functional; indeed, here we see that θ_2 slowly increases.

As a final remark, we note that in all of our computations, we employed a (damped) Newton iteration to solve the system of nonlinear equations arising from the discontinuous Galerkin discretization of the compressible Navier-Stokes equations. Within each Newton step, GMRES with Block-Gauss-Seidel preconditioning is exploited to solve the resulting linearized problem involving the Jacobian matrix, cf. [9], for further details. For each of the three mesh refinement algorithms employed above, the nonlinear solver proceeds as follows: starting on the coarsest mesh with free-flow conditions the nonlinear problem is solved by the Newton iteration described above. When the nonlinear residual converges below 10^{-8}, the mesh is refined once; then the discrete solution is interpolated onto the new mesh and is thereby taken as the starting solution for the Newton iteration on the newly refined mesh. In Table 2 we present the history of this solution process on a sequence of uniformly refined computational meshes; these results are also summarized in Fig. 2(a). On the coarsest mesh, with free-flow values, the Newton iteration requires a few steps until the iterative solution reaches the range of quadratic convergence. Indeed, after only 6 Newton steps the nonlinear residual is below the given tolerance of 10^{-8} and the mesh is refined; on subsequent meshes, the Newton iteration requires only 4 steps to reduce the residual below the given tolerance.

The convergence behaviour of the Newton iteration is analogous even when locally refined meshes are employed. Indeed, in Fig. 2(b) we plot the nonlinear residuals against the number of Newton steps employed for each of the meshes generated using the empirical error indicator. Here, we again see that on the first mesh 6 Newton steps are required to satisfy the convergence criterion, while only 4 are necessary on subsequent meshes. Analogous behaviour is also observed on the adaptive meshes generated using the weighted error indicator $|\eta_\kappa|$; for brevity, these results have been omitted.

References

1. Arnold, D, Brezzi, F., Cockburn, B., Marini, D. (2002): Unified analysis of discontinuous Galerkin methods for elliptic problems. SIAM J. Numer. Anal., **39(5)**, 1749–1779
2. Baumann, C.E., Oden, J.T. (1999): A discontinuous *hp* finite element method for the solution of the Euler and Navier–Stokes equations. Int. J. Numer. Meth. Fluids, **31**, 79–95
3. Bassi, F., Rebay, S. (1997): A high–order accurate discontinuous finite element method for the numerical solution of the compressible Navier–Stokes equations. J. Comput. Phys., **131**, 267–279
4. Becker, R., Rannacher R. (2001): An optimal control approach to a-posteriori error estimation in finite element methods. In: Iserles, A. (ed), Acta Numerica, pp. 1–102, CUP
5. Capon, P.J. (1995): Adaptive Stable Finite Element Methods for the Compressible Navier–Stokes Equations. Ph.D. Thesis, University of Leeds
6. Dolejsi, V. (2002): On the discontinuous Galerkin method for the numerical solution of the Euler and the Navier–Stokes equations. Int. J. Numer. Meth. Fluids, (submitted)
7. Dolejsi, V., Feistauer, M. Schwab, Ch. (2002): On discontinuous Galerkin methods for nonlinear convection–diffusion problems and compressible flow. Math. Bohem., **127(2)**, 163–179
8. Harriman, K., Houston, P., Senior, B., Süli, E. (2003): *hp*–Version discontinuous Galerkin methods with interior penalty for partial differential equations with nonnegative characteristic form. In: Shu, C.-W., Tang, T., Cheng, S.-Y. (eds), Recent Advances in Scientific Computing and Partial Differential Equations. Contemporary Mathematics, **330**, 89–119
9. Hartmann, R. (2004): The role of the Jacobian in the adaptive discontinuous Galerkin method for the compressible Euler equations. In: Warnecke, G. (ed), Analysis and Numerical Methods for Conservation Laws, Springer–Verlag (submitted)
10. Hartmann, R., Houston, P. (2002): Adaptive discontinuous Galerkin finite element methods for nonlinear hyperbolic conservation laws. SIAM J. Sci. Comp., **24(3)**, 979–1004
11. Hartmann, R., Houston, P. (2002): Adaptive discontinuous Galerkin finite element methods for the compressible Euler equations. J. Comp. Phys., **183**, 508–532
12. Numerical Simulation of Compressible Navier-Stokes Equations-External 2D Flows Around a NACA0012 Airfoil. GAMM Workshop, Dec. 4-6, 1985, Nice, France (Edt. INRIA, Centre de Rocquefort, de Rennes et de Sophia-Antipolis, 1986)
13. Süli, E., Houston, P. (2002): Adaptive finite element approximation of hyperbolic problems. In: Barth, T., Deconinck, H.(eds) Error Estimation and Adaptive Discretization Methods in Computational Fluid Dynamics. Lecture Notes in Computational Science and Engineering, Volume 25, pp. 269-344, Springer-Verlag